An artificial neural network model in predicting VTEC over Central Anatolia in Turkey

Ali Özkan

Osmaniye Korkut Ata University, Osmaniye Vocational School, 80000, Osmaniye, Turkey

E-mail address: aliozkan@osmaniye.edu.tr

Abstract

In this research, the capability of the artificial neural networks to predict GPS VTEC has been investigated over Central Anatolia in Turkey. The VTEC dataset was derived from the 19 permanent GPS stations belonging to TUSAGA-Aktif and IGS networks in the region. The study region extends in the area from west to east bounded by longitudes of 36.2°E-37.5°E and from south to north bounded by latitudes of 36.0°N-42.0°N. Considering the factors inducing VTEC variations in the ionosphere, an artificial neural network was herein proposed that has seven input neurons in a multi-layer perceptron model. The KURU and ANMU permanent GPS stations from TUSAGA-Aktif network were selected to implement the neural network model proposed. Based on the RMSE results achieved in the simulation tests with 50 attempts, the hidden layer in the NN model was designed to have 37 neurons since the lowest RMSE was reached in this attempt. According to the correlation coefficients, absolute and relative errors in the proposed neural network model, the NN VTEC are quite well predicted in hourly and seasonal basis referring to the GPS VTEC. In addition, this paper demonstrated that the NN VTEC model provides better performance than the global IRI model presents. Regarding as the true value of this study, the ANMU station demonstrates better in fitting with the proposed NN model rather than KURU station in the station-based comparison.

Keywords: GPS, Total Electron Content, GPS VTEC, Artificial Neural Network

1. Introduction

The ionospheric variations occurring within upper Earth’s atmosphere is a complicated phenomena caused by solar activity such as flares and CMEs (Coronal Mass Ejections). Since the ionosphere has a dispersive feature, electromagnetic transmissions such as GPS (Global Positioning System) signals propagating through the ionosphere are exposed to delay. This delay is directly proportional to the TEC (Total Electron Content) of the ionosphere along the path of the signal. It is described that TEC is the total number of free electrons in a one-meter squared column projected along the signal path between the source on the satellite and the receiver on the Earth [1–3]. The unit of TEC is defined as TECU which equals to 10^{16} electrons/m^2 [3–7]. The slant path with respect to the local vertical at the position of GPS receiver extends to the satellite as a function of elevation angle. The STEC (slant TEC) calculated along the path of the GPS signal can be projected into the VTEC (vertical TEC) by using mapping function [5,8]. VTEC values vary from several to hundreds TECU due to solar cycle, geographical latitude and longitude, diurnal variations, seasonal variations, geomagnetic effects and seismic activities [9,10].

Nowadays, dual-frequency GPS receivers allow eliminating frequency-dependent refractions arising from dispersive nature of the ionosphere. Thanks to geometry free linear combination of L1 and L2 phase observables while using dual-frequency GPS receivers, it is possible to calculate ionospheric refractions. On the other hand, single-frequency GPS receivers are inadequate to deal with such ionospheric variations. In this case, global ionospheric models distributed by several organizations such as IGS CODE (International GNSS Service, Centre for Orbit Determination in Europe), ESA (European Space Agency), JPL (Jet Propulsion Laboratory), IRI (International Reference Ionosphere) can be alternative by interpolating TEC data nearest to the corresponding position of the GPS receiver [5,11–14].

Since both the GPS receivers on the ground are sparse to model regional grid of TEC and also global TEC models have limited accuracy, artificial neural networks are preferred for predictive modeling of ionosphere [15–19]. Not only ionospheric variations but also mean temperature predictions [20], solar radiation forecasting [21], meteorological predictions [22] or tropospheric estimations [23] were recently studied using neural network models to better interpret the geophysical processes over the Earth. On the other hand, the spatial and time-dependent components of the ionospheric activity need to be considered to predict VTEC variations in high spatial and temporal accuracy [18, 24, 25]. Okoh et al. [18], Homam [24] and Mallika et al.

[25] investigated the neural network performances in terms of VTEC predictions associated with the spatio-temporal contributors over Equatorial Region. Homam [24] adopted a data acquisition methodology related to the occurrence of ionopheric scintillation over a GPS station in Malaysia in order to integrate into neural network modeling for VTEC predictions. Okoh et al. [18] argued about the effectiveness of the foF2 storm model derived from IRI products, in which it was used as an additional neuron for the neural input layer in their study over Nigeria. Mallika et al. [25] investigated the performance of the neural networks in predicting VTEC variations over India using dense global dataset of IRI models, contrarily limited ground-based observations for neural network training and model testing. In this study, it is aimed to predict significant GPS VTEC based on artificial neural network modeling using dense GPS observations obtained from permanent stations within a regional subnetwork over Central Anatolia in Turkey. The neural network model proposed here depends on a station-based approach, which contains network training by using a bulk of GPS data acquired from 19 permanent stations for the period of 2015-2019 and validation of NN VTEC predictions in 2020 with respect to the GPS VTEC and IRI2012 VTEC at the two northernmost and southernmost GPS stations, KURU and ANMU, in the Mid-Latitude Region.

2. Materials and methods

2.1. GPS dataset and analysis

GPS data processed within the scope of this study were obtained from the TUSAGA-Aktif (Turkish National Permanent GPS Network-Active) and IGS networks over Central Anatolia in Turkey (Figure 1). The RINEX (Receiver Independent Exchange Format) files with 30 seconds measurement interval in the 24 hours of observation span were downloaded from the IGS [26] and TUSAGA-Aktif [27] websites. The GPS network consisting of 19 permanent stations covers an area from 36.2°E to 37.5°E in longitudes and 36.0°N to 42.0°N in latitudes. Supplementary Table S1 summarizes the detailed descriptions about the permanent GPS stations. The GPS dataset was generated by selecting specific daily GPS observations in the range of years for 2015-2020.

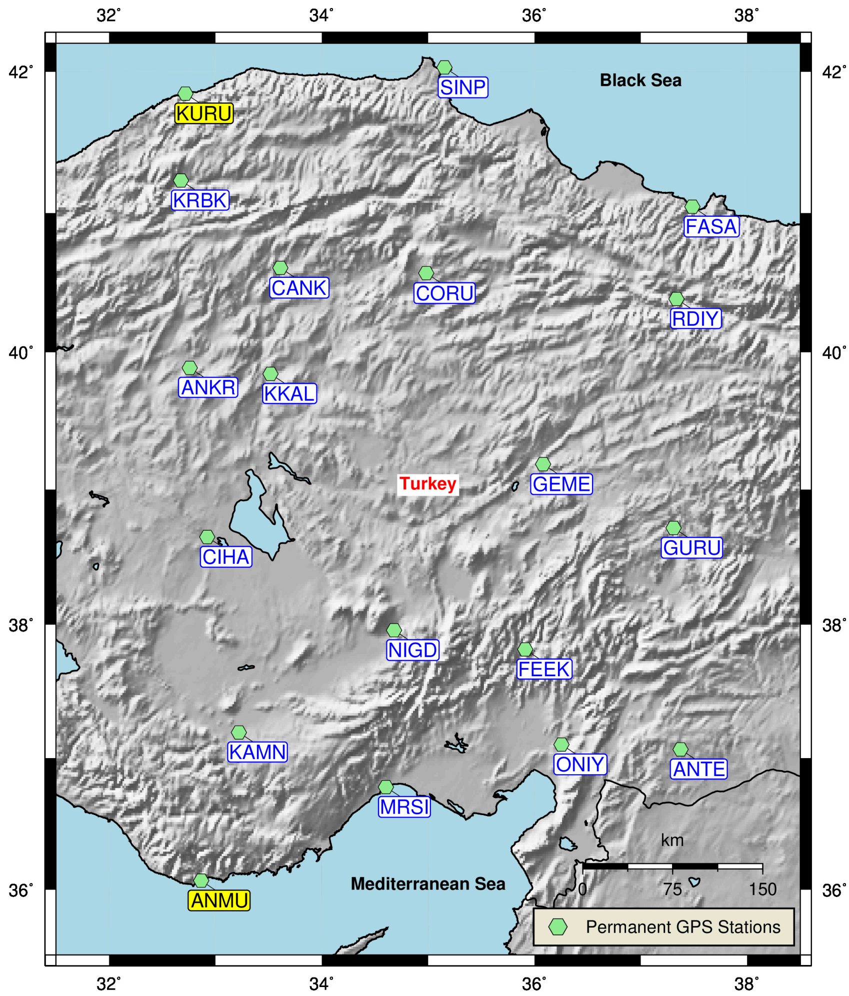

Figure 1. GPS network at the central region of Turkey used in this study.

In order to derive the total electron content at the locations of permanent stations, GPS data were processed using the GPS-TEC analysis (Ver. 3.0) software developed by Gopi Krishna Seemala [28]. The software calculates STEC along the slant trajectory. It has also the capability for processing cycle slips in phase observations, reading satellite biases from DCB (Differential Code Bias) files downloaded from IGS CODE, calculating the receiver bias and inter-channel biases for different satellites in the receiver and plotting the VTEC values as well. The STEC along the slant trajectory can be extracted from the geometry-free linear combination of GPS observations as per following Eq. (1) [29]:

$$\boldsymbol{STEC} = \frac{f_1^2 \cdot f_2^2}{40.3082\,\frac{m^3}{s^2} \cdot (f_1^2 - f_2^2)} \{(\boldsymbol{P_2} - \boldsymbol{P_1}) - (\boldsymbol{b_P^s} + \boldsymbol{b_P^r})\} \tag{1}$$

where; P_1 and P_2 are pseudorange observables corresponding to the high *(f_1=1575.42 MHz)* and low *(f_2=1227.6 MHz)* GPS frequencies respectively, $b^s{}_P$ is the pseudorange satellite delay and b^{r}_{P} is the pseudorange receiver delay. However, the STEC must be then converted to the VTEC considering a spherical thin-shell model for the ionosphere. According to the SLM (single layer model), a very thin layer at a fixed height above the Earth's surface contains all the free electrons [6].

Thus, as given in following equations, VTEC at ionospheric pierce point is derived using a mapping function [7,30,31] based on the SLM:

$$STEC = VTEC \,.\, M(z) + (b_s + b_r + b_{rx}) \tag{2}$$

with

$$M(z) = \frac{1}{\cos z^1} = \frac{1}{\sqrt{1 - sin^2 z^1}} \tag{3}$$

$$\sin z^1 = \frac{R}{R+H} \,.\, \sin z \tag{4}$$

where; *M(z)* is the mapping function, *R* is the Earth's mean radius, b_s is satellite bias, b_r is receiver bias, b_{rx} is receiver interchannel bias, *H* is the ionospheric layer height, *z* and *z′* are the zenith angles at the receiver site and at the ionospheric pierce point, respectively. In this study, the ionospheric layer was assumed at a fixed height of 350 km above the Earth's surface. In addition, the sampling rate of each GPS receiver was 30 seconds and the minimum elevation angle criterion was assumed to be 30º in case any multipath effects might distort the GPS observations.

2.2. Artificial Neural Network Approach

Neural networks are regarded as artificial intelligence mechanisms that can be trained and are able to learn to deal with non-linear input/output relationships in the complicated processes [32,33]. The mechanism contains simple processing elements named as artificial neurons, in which the summation provided by manipulating the input signal using weights is stored. The determination of the weights of the input signal in an artificial neural network is realized by an iterative adjustment procedure during the training process until the optimum weights are achieved [34]. Once the neural network is trained, the input signal passes through an activation function (transfer function) to generate output of neurons. Sigmoid activation function given in Eq. (5) is usually preferred as activation function in multi-layer perceptron model.

$$\boldsymbol{f(x) = \frac{1}{1 + e^{-x}}} \tag{5}$$

The activation function serves as non-linear filter to generate output signal. During the training stage, a back-propagation algorithm is applied in feed-forward and feed-backward processes. In an iterative approach, the biases of the neural network are adjusted repeatedly until the RMSE (root mean square error) reaches a threshold value for the output signal. In this study, the activation function of all layers is the sigmoid function and Levenberg-Marquardt back-propagation algorithm was applied to train the network.

Due to its quick response for predictions and effectiveness during training process, the multi-layer perceptron neural network consisting of one input layer, one hidden layer with many neurons and one output layer was preferred in this study. The optimal number of neurons and layers can be decided in consequence of trial and error as per each specific problem [35]. The strategy followed here to determine the optimal number of neurons in hidden layer was realized using different neural network designs with varying input neurons. Since VTEC is associated with the solar cycle variations, seasonal variations, diurnal variations, spatial variations and solar activity variations, the proposed neural network herein was anticipated to learn considering those parameters. The data about the sunspot numbers were provided from the website of World Data Center Sunspot Index and Long-term Solar Observations [36]. Additionally, the relationship between VTEC and electron density at F2 peak (NmF2) has a strong positive correlation [37,38] so that the learning stage of the network was considered to be more effective by incorporation of the NmF2 data obtained from the IRI model [39]. Furthermore, the IRI is an empirical ionospheric model that introduces reliable global data accompanying with long-term solar cycle variations [18]. Accordingly, the input layer of our neural network contains seven neurons namely year, day of the year, hour of the day, latitude, longitude, sunspot number and electron density at F2 peak (Figure 2).

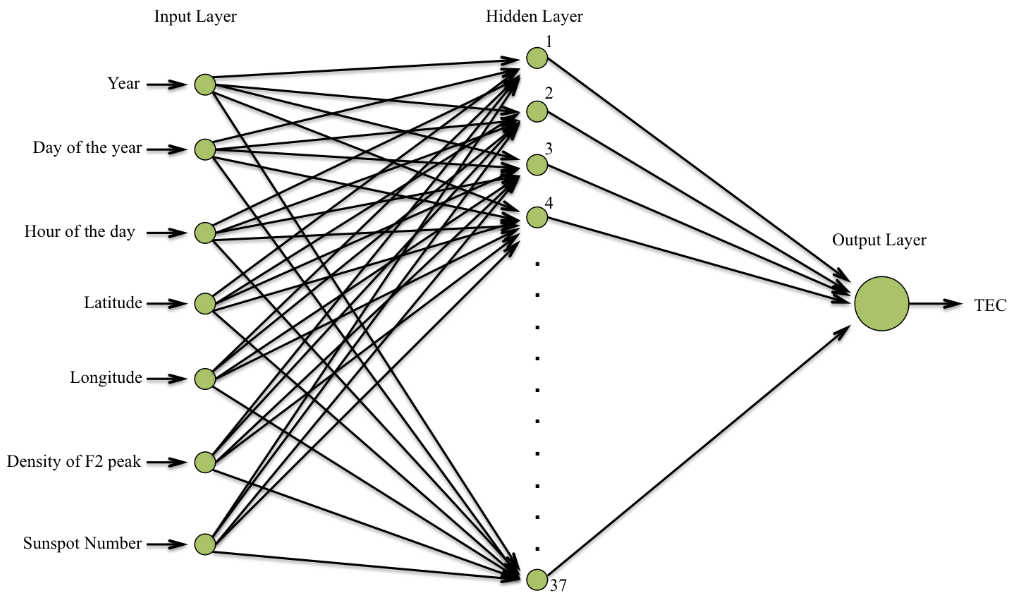

Figure 2. The structure of the multi-layer perceptron neural network with one hidden layer used in this research.

Using the different combinations of input neurons, several network designs were statistically tested for the determination of the optimal architecture of the neural network. The different neural networks were designed from the simplest structure to more complex one, in which varying parameters and numbers of input neurons were considered (Figure 3).

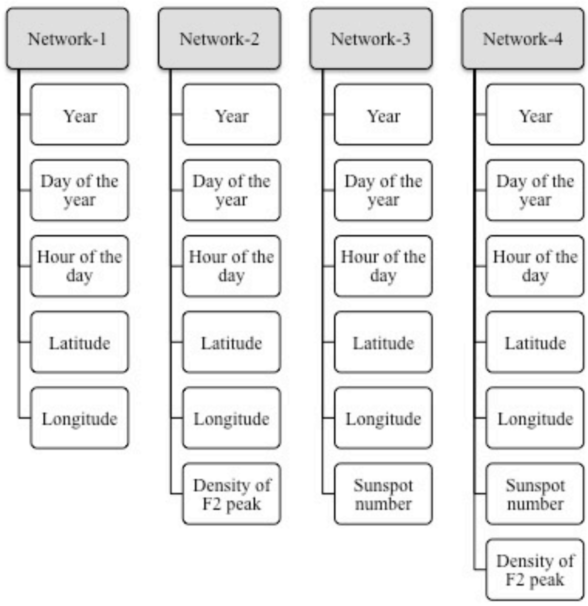

Figure 3. The different neural network designs with the corresponding input neurons in each.

Considering a test procedure to determine which network design was the most appropriate for network training, each of four network designs was simulated 50 times in terms of varying numbers of neurons in the hidden layer. The decision criterion of the testing procedure was the RMSE parameter statistically expected to be the lowest based on the predictions in the neural networks [40].

The analyses within this research covers the period between 2015 and 2020. The strategy to constitute a dataset was adopted by selecting the days with the weakest ionospheric activity for each month. Hourly-averaged VTEC values calculated from GPS observations were the output signal of the neural network. It is worth to say that the training dataset differs from the dataset used in the random model testing. In the random testing, the proposed model has been assessed in terms of the temporal performance. The dataset for the period of 2015-2019 was acquired from all the permanent stations performing in the GPS network demonstrated in Figure 1 and allocated to training by 70% of it, validation by 15% of it and testing by 15% as of remaining. This training dataset was randomly selected among the daily GPS data acquired in those permanent GPS stations during the weakest day of each month in a year, which means that each station provides data of 4 out of 12 random weakest days in a year. Apart from this dataset used to train the neural network, the GPS data for the year of 2020 acquired from KURU (41.846ºN, 32.718ºE) and ANMU (36.069ºN, 32.865ºE) permanent stations were randomly used to test the neural network model. There were two criteria for the data selection in random testing stage, as one of them was to use the data out of the training dataset period, which were 2020 GPS data here and the other was choosing the northernmost and the southernmost stations to compare the station-based predictions. In addition, the diurnal performance of the neural network was tested for different times of a day namely 03:00 UTC (Coordinated Universal Time) equivalent to 06:00 Local Time, 09:00 UTC (12:00 Local Time), 15:00 UTC (18:00 Local Time) and 21:00 UTC (00:00 Local Time), which correspond to near the time of sunrise, the noontime with high ionospheric level, near the time of sunset and the midnight, respectively. Besides, in order to test the seasonal performance of the neural network, the predictions were also tested for different seasons in 2020 namely vernal equinox, summer solstice, autumnal equinox and winter solstice.

The performance of our neural network was assessed in terms of the absolute and relative errors estimated using following equations, respectively:

$$|\boldsymbol{E_{abs}}| = |\boldsymbol{TEC_{NN}} - \boldsymbol{TEC_{GPS}}| \tag{6}$$

$$|\boldsymbol{E_{rel}}| = \left(\frac{|\boldsymbol{E_{abs}}|}{\boldsymbol{TEC_{GPS}}}\right) \boldsymbol{x\ 100} \tag{7}$$

where; E_{abs} is the absolute error, E_{rel} is the relative error, TEC_{NN} and TEC_{GPS} are predicted VTEC by the neural network and GPS-derived VTEC, respectively [19,41,42]. In this context, the less the absolute and relative errors, the closer the predicted VTEC values by neural network model and calculated VTEC values from GPS observations.

3. Results and discussions

First, in order to determine the optimum architecture of the neural network, all the proposed neural network designs were compared based on the RMSEs for the dataset period between 2015 and 2019. In this research, the RMSEs indicating the deviations of predicted VTEC by the neural network (hereinafter referred to as NN VTEC) from observed VTEC by means of GPS (hereinafter referred to as GPS VTEC) were calculated per the number of neurons in hidden layer for each network designs individually. Both in Figure 4 and Figure 5, it is evidently proven that the Net4 consisting of seven input neurons namely the year, day of the year, hour of the day, latitude, longitude, sunspot number, density of F2 peak neurons has the lowest RMSE compared to other three network designs. The RMSE for the dataset of KURU and ANMU stations has the minimum value (~1.2 TECU) for the simulation test using 37 neurons in the hidden layer, which indicates the best agreement between the NN VTEC and GPS VTEC (Figure 5). Thus, the training of the network was achieved using seven neurons in the input layer and 37 neurons in the hidden layer.

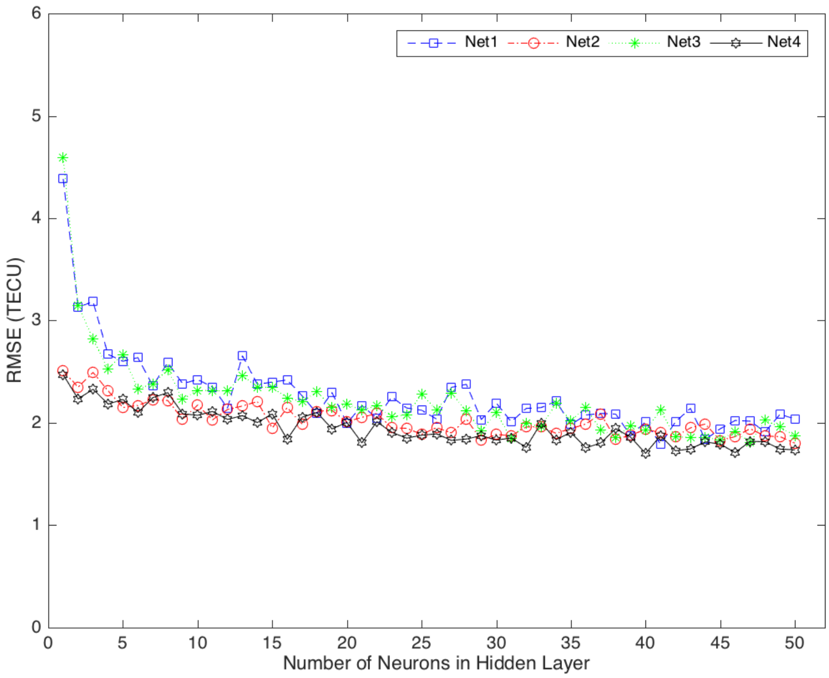

Figure 4. The RMSEs using the random dataset for the period between 2015 and 2019.

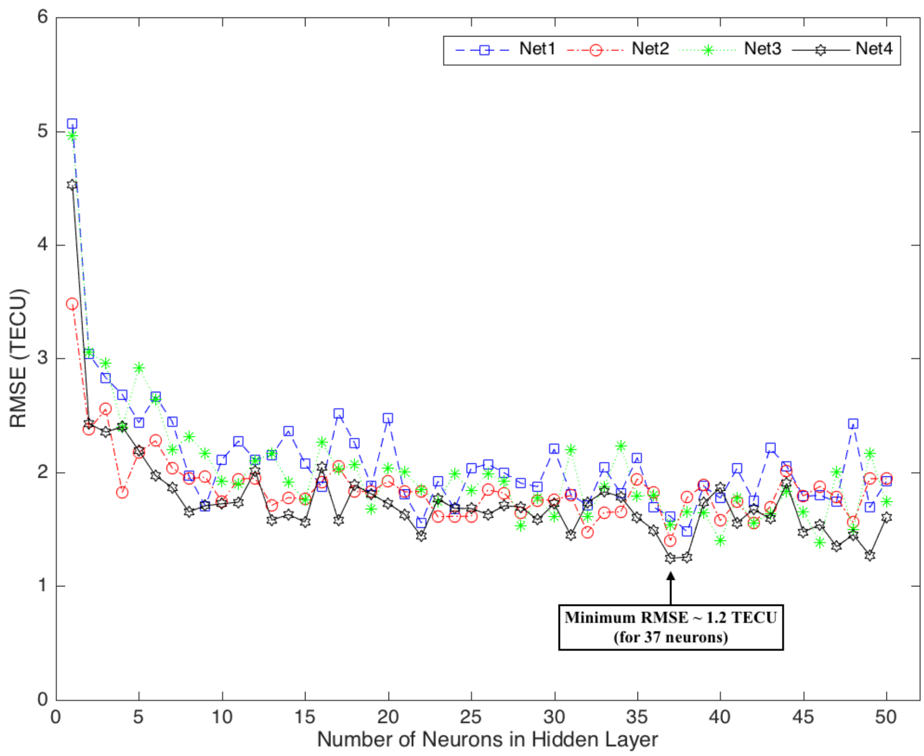

Figure 5. The RMSEs using the dataset of KURU and ANMU stations for the period between 2015 and 2019.

Besides, it is clear that the higher the RMSE, the worst the neural network design performance. The first neural network design (Net1) has the highest RMSEs compared to other network designs that means the fewer input neurons in, the poorer the network performance. Furthermore, the second (Net2) and third (Net3) neural network designs have moderate performances compared to the Net1 (the worst) and the Net4 (the best). As a result, the increase in the number of input neurons helps the neural network to learn better and to make more reasonable predictions.

In Figure 6 and Figure 7, the NN VTEC (prediction in the vertical axis) versus the GPS VTEC (target in the horizontal axis) was plotted for KURU and ANMU stations for the 2020 dataset, respectively. The scatter plots for the predictions and their corresponding targets demonstrate the red lines of best fitting for regression model together with the correlation coefficients (r).

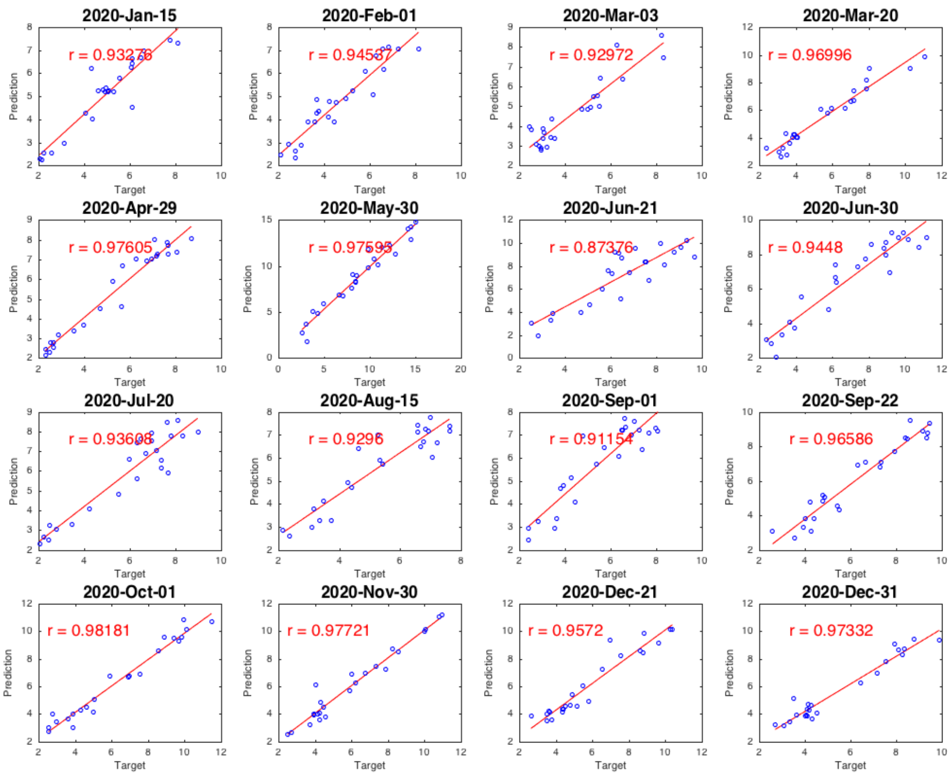

Figure 6. The correlations between the NN VTEC and the GPS VTEC for the 2020 dataset over KURU station.

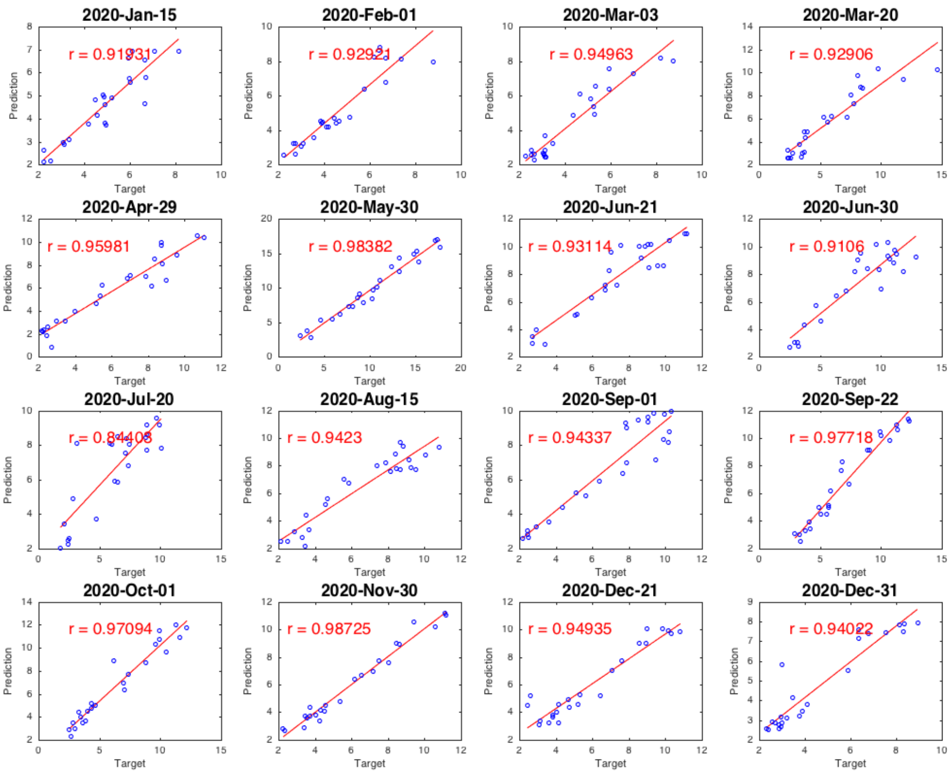

Figure 7. The correlations between the NN VTEC and the GPS VTEC for the 2020 dataset over ANMU station.

It is a fact that there is a high correlation between NN VTEC and GPS VTEC since all the correlation coefficients except the lowest two are above 0.9 for both KURU and ANMU stations. The lowest correlation coefficients were 0.87376 for KURU station in June 21, 2020 and 0.84408 for ANMU station in July 20, 2020.

In order to evaluate the diurnal performance of the neural network, NN VTEC was compared with the corresponding GPS VTEC for the specific times of the day during 2020 over KURU and ANMU stations. These times within the day were determined based on the positions of the sun with respect to the local during the day as the near the time of sunrise, the noontime with high ionospheric level, near the time of sunset and the midnight. Thus, 03:00 UTC (06:00 Local Time), 09:00 UTC (12:00 Local Time), 15:00 UTC (18:00 Local Time) and 21:00 UTC (00:00 Local Time) were considered as the benchmarks for intraday variations. The local time in Turkey is 3 hours ahead of the universal time.

The NN VTEC obtained from the neural network model and GPS VTEC calculated from the GPS observations were compared in hourly basis for those specific times of the day during 2020 over KURU and ANMU stations (Figure 8 and Figure 9).

Additionally, the absolute and relative errors of NN VTEC from GPS VTEC for those specific times of the day during 2020 over KURU and ANMU stations were demonstrated, respectively, in Supplementary Figure S1-S4. From those figures, it is evident that the predictions (NN VTEC) for the specific times of the day during 2020 are highly correlated with the targets (GPS VTEC) since the highest absolute errors does not exceed the value of 2.5 TECU during 2020 over both stations.

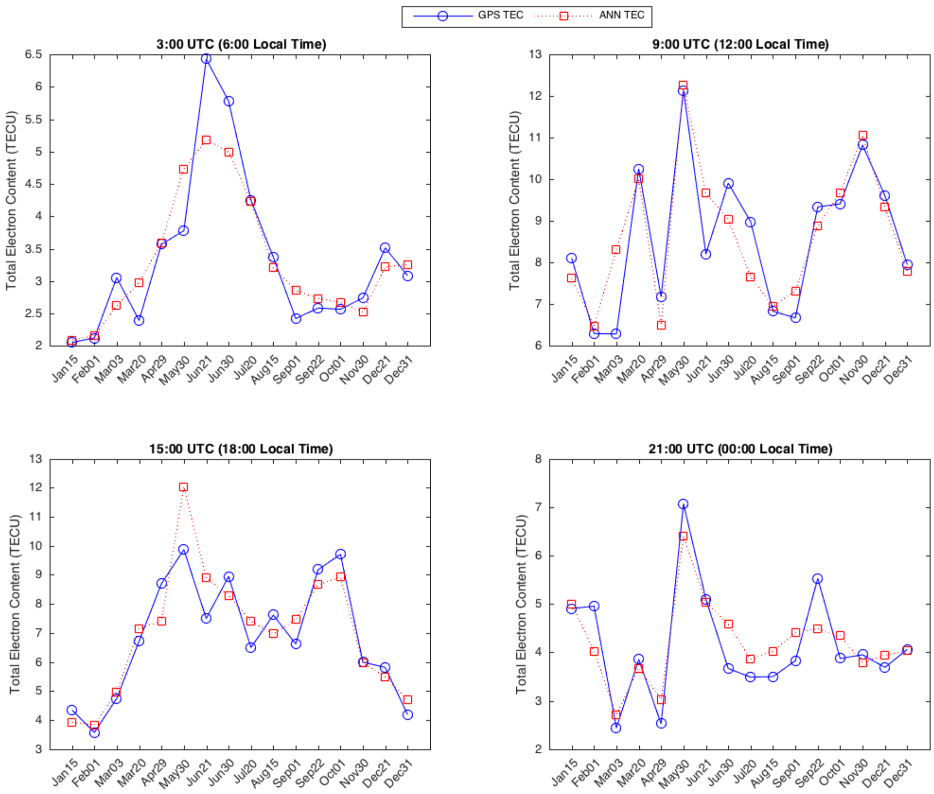

Figure 8. Hourly comparison of NN VTEC and GPS VTEC for the specific times of the day during 2020 over KURU station.

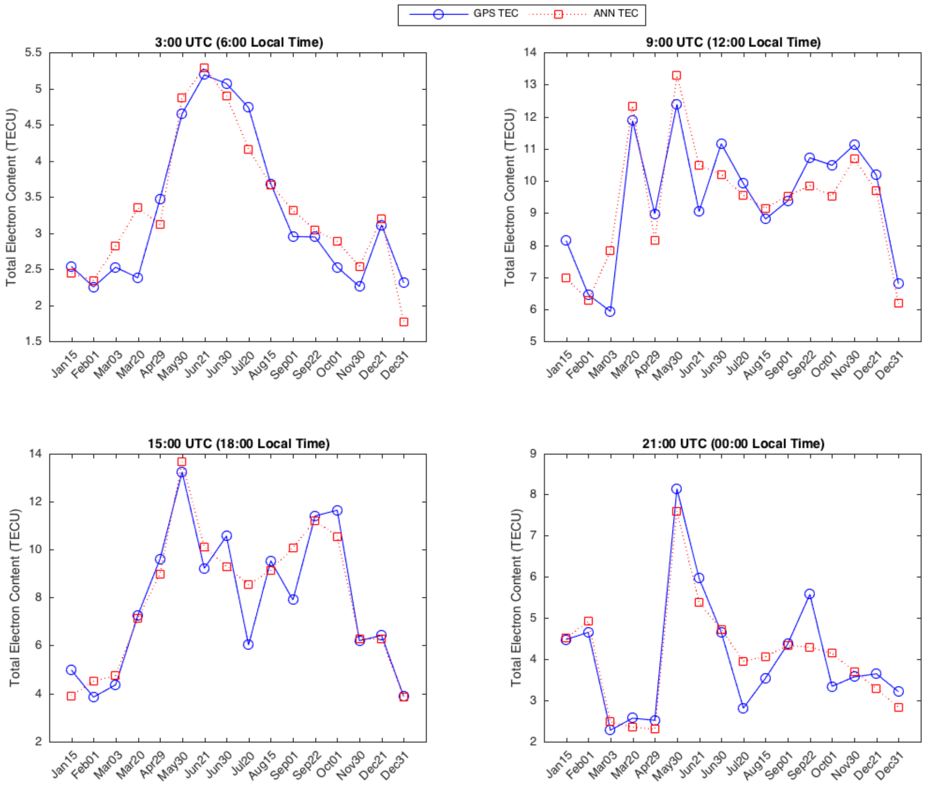

Figure 9. Hourly comparison of NN VTEC and GPS VTEC for the specific times of the day during 2020 over ANMU station.

Table 1. The correlation coefficients for the comparison of the specific day times

Station	03:00 UTC	09:00 UTC	15:00 UTC	21:00 UTC
KURU	0.91149	0.87642	0.85907	0.91008
ANMU	0.93391	0.89154	0.93463	0.92716

As seen from the upper-left plots in Figure 8 and Figure 9, the NN VTEC and GPS VTEC at 03:00 UTC (06:00 Local Time) over both KURU and ANMU stations have mostly similar trends during 2020 indicating good predictions for the GPS VTEC. The correlation coefficients between NN VTEC and GPS VTEC at 03:00 UTC (06:00 Local Time) are 0.91149 and 0.93391 over KURU and ANMU stations, respectively (Table 1). In Supplementary Figure S1 and Figure S2, it is noticed that the absolute errors at 03:00 UTC (06:00 Local Time) over KURU station are less than 1 TECU except the error only on June 21, 2020. On the other hand, the absolute errors at 03:00 UTC (06:00 Local Time) over ANMU station are less than 1 TECU throughout the year. Accordingly, the maximum relative errors at 03:00 UTC (06:00 Local Time) reached to 25% and 40% over KURU and ANMU stations, respectively (Suppl. Figure S3 and Figure S4).

At 09:00 UTC (12:00 Local Time) presented in the upper-right plots in Figure 8 and Figure 9, the NN VTEC and GPS VTEC demonstrate quite similar variations during 2020 over both KURU and ANMU stations. Compared to at 03:00 UTC (06:00 Local Time), the NN VTEC and GPS VTEC gives lower correlation coefficients at 09:00 UTC (12:00 Local Time) as 0.87642 over KURU station and 0.89154 over ANMU station (Table 1). The absolute errors at this time of the day slightly exceed the limit of 1 TECU on March 03, June 21 and July 20 over KURU station while the exceeding of 1 TECU absolute errors are on January 15, March 03 and June 21 over ANMU station (Suppl. Figure S1 and Figure S2). The highest absolute errors at 09:00 UTC (12:00 Local Time) within 2020 are faintly close to the limit of 2 TECU over those stations. However, the trends of absolute errors over both stations indicate decreases towards the end of 2020. The maximum relative errors at 09:00 UTC (12:00 Local Time) on both stations exceed the limit of 30% on March 03, 2020 (Suppl. Figure S3 and Figure S4).

At 15:00 UTC (18:00 Local Time) presented in the lower-left plots in Figure 8 and Figure 9, the variations of NN VTEC and GPS VTEC are fairly correlated although some predictions does not fit well enough to GPS VTEC. The NN VTEC on May 30 over KURU station, the NN VTEC on July 20 and September 01 over ANMU station indicate poorest predictions in the neural network model. The correlation coefficient between NN VTEC and GPS VTEC at 15:00 UTC (18:00 Local Time) is 0.85907 for KURU, the lowest of the day for that station, although the correlation coefficient between these variables is 0.93463 for ANMU, the highest of the day for that station (Table 1). The absolute errors at 15:00 UTC (18:00 Local Time) over each stations reach to the highest by exceeding the limit of 2 TECU among all the predictions in the model (Suppl. Figure S1 and Figure S2). The relative errors at 15:00 UTC (18:00 Local Time) are less than 25% over KURU station (Suppl. Figure S3) while the relative errors over ANMU station reach at the maximum by exceeding the limit of 40% on July 20, 2020 (Suppl. Figure S4).

The predictions for NN VTEC at 21:00 UTC (00:00 Local Time) in the lower-right in Figure 8 and Figure 9 demonstrate the relatively smooth variations compared to the GPS VTEC over both stations. The NN VTEC and GPS VTEC at 21:00 UTC (00:00 Local Time) indicate the goodness of fitting with the correlation coefficient of 0.91008 and 0.92716 over KURU and ANMU stations, respectively (Table 1). The highest absolute errors at 21:00 UTC (00:00 Local Time) for both KURU and ANMU station are between 1.0-1.5 TECU on September 22, 2020 (Suppl. Figure S1 and Figure S2). The maximum relative error at 21:00 UTC (00:00 Local Time) is less than 25% for KURU station although it exceeds the limit of 40% on July 20, 2020 for ANMU station (Suppl. Figure S3 and Figure S4).

On the other hand, another perspective in evaluating the performance of the neural network is based on the seasonal variations of VTEC. Thus, the different seasons in 2020 namely vernal equinox, summer solstice, autumnal equinox and winter solstice were considered to investigate the seasonal variations. In the seasonal evaluation process, the IRI2012 VTEC derived from IRI2012 model using NeQuick parameter for the Ne topside was also incorporated into the analysis in order to compare the neural network model with an international reference model. Accordingly, the seasonal comparison of the NN VTEC with the GPS VTEC and the IRI2012 VTEC was demonstrated in Figure 10 and Figure 11. As expected, it is very clear that the NN VTEC provides much better correlation with the GPS VTEC than the IRI2012 VTEC has. The maximum correlations between the NN VTEC and the GPS VTEC are in autumnal equinox as the coefficients of 0.96560 over KURU station and 0.98680 over ANMU station (Table 2). However, the IRI2012 VTEC and GPS VTEC have the maximum correlations in winter solstice with the correlation coefficients of 0.94949 for KURU station and 0.96866 for ANMU station. On the contrary, the minimum correlations indicate to summer solstice in all the seasons during 2020. The minimum correlation coefficients between NN VTEC and GPS VTEC are 0.92844 for KURU station and 0.92746 for ANMU station. Similarly, the minimum correlation coefficients between IRI2012 VTEC and GPS VTEC are 0.85616 for KURU station and 0.90834 for ANMU station. The absolute errors during each season are also shown in Supplementary Figure S5 and Figure S6. As seen from those figures, the NN VTEC has very few absolute errors of TECU from GPS VTEC compared to the absolute errors of the IRI2012 VTEC during all seasons in 2020. The absolute errors, as well as the correlation coefficients, demonstrate better agreement between the NN VTEC and GPS VTEC during all seasons rather than IRI2012 VTEC. As similar to the relatively poorer correlation coefficients of the NN VTEC in the summer solstice, the NN VTEC has also the highest absolute errors for the same season over both KURU and ANMU stations. However, the NN VTEC for the rest of the seasonal times in 2020 has quite low absolute errors as a few TECU at most over both stations. On the other hand, despite the relatively high correlation coefficients in the vernal equinox, the IRI2012 VTEC reaches the highest absolute errors exceeding the limit of 35 TECU during the noontime in the vernal equinox over both KURU and ANMU stations. From the Supplementary Figure S5 and Figure S6, it is also obvious that the IRI2012 VTEC provides the best performance during the winter solstice over both stations, which confirms the highest correlation coefficients.

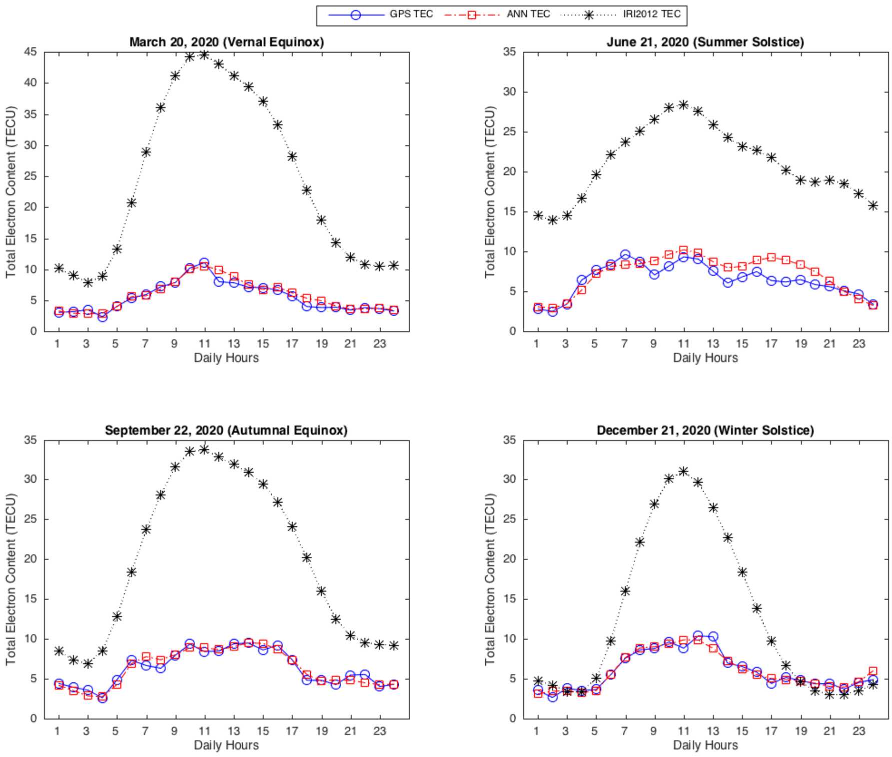

Figure 10. The seasonal comparison of the NN VTEC and the IRI2012 VTEC with the GPS VTEC during 2020 over KURU station.

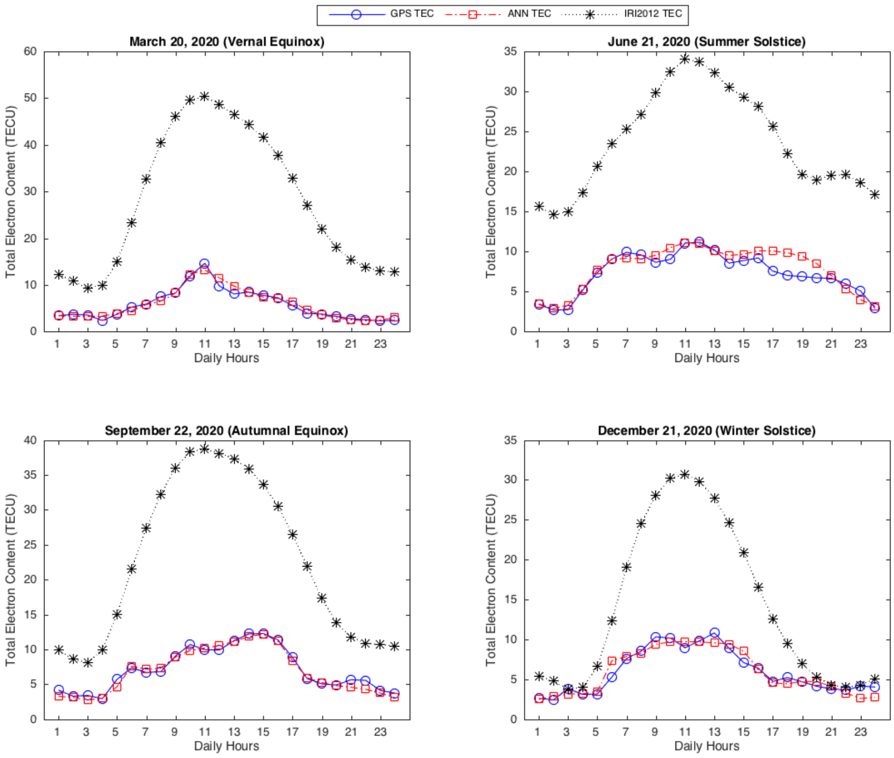

Figure 11. The seasonal comparison of the NN VTEC and the IRI2012 VTEC with the GPS VTEC during 2020 over ANMU station.

Table 2. The correlation coefficients for the comparison of seasonal variations.

Station Code	**Model**	**Vernal Equinox (March 20)**	**Summer Solstice (June 21)**	**Autumnal Equinox (September 22)**	**Winter Solstice (December 21)**
KURU	NN VTEC	0.95349	0.92844	0.96560	0.96070
	IRI2012 VTEC	0.94893	0.85616	0.91466	0.94949
ANMU	NN VTEC	0.97437	0.92746	0.98680	0.95510
	IRI2012 VTEC	0.91737	0.90834	0.91173	0.96866

The station-based comparison of the neural network model can give some significant indications about the spatial contributions of the GPS network for predictions. For this purpose, the GPS stations were individually compared with the other in terms of the TECU predictions, absolute and relative errors in the neural network during different times of the day in order to reveal the diurnal performance of the each station (Figure 8, Figure 9, Suppl. Figure S1-Figure S4). During the day, the ANMU station provides better agreement with the neural network model than the KURU station as also confirmed by the correlation coefficients (Table 1). On the other hand, the seasonal individual performances of the stations were comparably evaluated during different seasons in the year using the TECU predictions and absolute errors in the neural network (Figure 10, Figure 11, Suppl. Figure S5 and Figure S6). During the equinox seasons in 2020, the ANMU station gives better performance with the neural network model than the KURU station as likewise verified by the correlation coefficients (Table 2). During the summer solstice, the absolute errors in ANMU station are relatively lower than the ones in KURU station although the correlations are statistically in the same level. However, during the winter solstice, the KURU station provides slightly better performance than the ANMU station.

4. Conclusions

The GPS data obtained from the TUSAGA-Aktif and IGS networks over the Central Anatolia in Turkey was used as the output of this research. The GPS network consisting of 19 permanent stations provided also random data for the training of the neural network. The neural network structure was established using the seven input neurons namely year, day of the year, hour of the day, latitude, longitude, sunspot number and electron density at F2 peak. The optimal numbers of the input neurons and the neurons in the hidden layer were determined as per the simulation tests aimed to reach the lowest RMSE. The neural network design with seven input neurons (Net4) verified the lowest RMSE compared to the other network designs. The simulation tests demonstrated that the more input neurons integrated into the input layer, the better the network training and the more significant the predictions. Furthermore, after training process, the hidden layer comprising of 37 neurons was integrated into the neural network as giving the best performance. Additionally, the target GPS dataset for the neural network model has here played pivotal role. Unlike the targets used in the network training, it was aimed to achieve a network validation process using unique independent targets in the model testing. Thus, the target dataset was divided into two categories. The one for network training contains random GPS data acquired from 19 permanent stations during the period of 2015-2019. On the contrary, the model testing was accomplished by using a different bulk of targets calculated from the GPS observations in 2020. From this perspective, some significant indicators prove the applicability of the proposed model such that the correlations between the predictions for the NN VTEC and their corresponding targets for GPS VTEC have pointed out quite well fitting at the selected days in 2020. Those selected days were determined as per the weakest ionospheric activity within each month during the year. According to the station-based model proposed in this study, the predictions have been validated at the northernmost and southernmost stations namely KURU and ANMU, respectively. Using this multi-layer perceptron model, the diurnal variations of VTEC can be predicted quite well by the proposed neural network structure at the specific day times since the absolute and relative errors in TECU are very low. The correlation coefficients also simply demonstrate well fitting for diurnal predictions, indicating that the different day times are not deterrent in the modeling. The testing GPS stations were compared with each other in the hourly basis of diurnal variations. The ANMU station provides better predictions correlated with the proposed neural network model rather than the KURU station. It is also important to verify that the present-day diurnal variations can be predicted highly accurate whether for the northernmost or southernmost, regardless of the location in the study area. Besides, the station-based model proposed here allows revealing the seasonal variations of VTEC during different seasons in 2020 comparably at the two opposites. The seasonal performance of each station differs depending on the variations in the seasons of vernal equinox, summer solstice, autumnal equinox and winter solstice. Considering the correlation coefficients and the absolute errors of the NN VTEC from the GPS VTEC, the seasonal comparison of the NN VTEC with the GPS VTEC notices the high accurate prediction capability of the neural network model during different seasons in 2020. During equinox seasons, the ANMU station evidently demonstrates better in fitting with the proposed neural network while the KURU station outperforms during summer and winter solstices. As also expected, during the all seasons in 2020, the NN VTEC provides better predictions for the seasonal variations than the IRI2012 VTEC obtained from the global IRI model. To conclude, instead of competing with the global models like IRI, the proposed model in this study is there to elaborate the power of such neural network models in predicting the VTEC since those models could be a well contributor to improve the regional models.

Declaration of Competing Interest

The author declares that he has no known competing financial interests or personal relationships that could have appeared to influence the work reported in this paper.

References

[1] Y. Huang, K. Cheng, S. Chen, On the equatorial anomaly of the ionospheric total electron content near the northern anomaly crest region, Journal of Geophysical Research: Space Physics. 94 (1989) 13515–13525.

[2] R.G. Rastogi, J.A. Klobuchar, Ionospheric electron content within the equatorial F 2 layer anomaly belt, Journal of Geophysical Research: Space Physics. 95 (1990) 19045–19052.

[3] B. Hofmann-Wellenhof, H. Lichtenegger, J. Collins, Global positioning system: theory and practice, Springer Science & Business Media, 2012.

[4] G. Seeber, Satellite Geodesy: Foundations, Methods and Applications, International Hydrographic Review. 4 (2003) 92–93.

[5] S. Schaer, Mapping and predicting the Earth's ionosphere using the Global Positioning System, Ph.D. Thesis, Astronomical Institute, University of Bern. (1999).

[6] U. Wild, Ionosphere and geodetic satellite systems: permanent GPS tracking data for modelling and monitoring., Geod.-Geophys. Arb. Schweiz. 48 (1994).

[7] A.J. Mannucci, B.D. Wilson, C.D. Edwards, A New Method for Monitoring the Earth's Ionospheric Total Electron Content Using the GPS Global Network, in: Proceedings of the 6th International Technical Meeting of the Satellite Division of The Institute of Navigation (ION GPS 1993), 1993: pp. 1323–1332.

[8] J.S. Shim, Analysis of total electron content (TEC) variations in the low-and middle-latitude ionosphere, Ph.D. Thesis. (2009).

[9] R. Warnant, E. Pottiaux, The increase of the ionospheric activity as measured by GPS, Earth, Planets and Space. 52 (2000) 1055–1060.

[10] G. Liu, W. Huang, J. Gong, H. Shen, Seasonal variability of GPS-VTEC and model during low solar activity period (2006-2007) near the equatorial ionization anomaly crest location in Chinese zone, Advances in Space

Research. 51 (2013) 366–376. https://doi.org/10.1016/j.asr.2012.09.002.

[11] D. Bilitza, D. Altadill, Y. Zhang, C. Mertens, V. Truhlik, P. Richards, L.-A. McKinnell, B. Reinisch, The International Reference Ionosphere 2012–a model of international collaboration, Journal of Space Weather and Space Climate. 4 (2014) A07.

[12] S.K. Leong, T.A. Musa, K. Omar, M.D. Subari, N.B. Pathy, M.F. Asillam, Assessment of ionosphere models at Banting: Performance of IRI-2007, IRI-2012 and NeQuick 2 models during the ascending phase of Solar Cycle 24, Advances in Space Research. 55 (2015) 1928–1940.

[13] R. Scharroo, W.H.F. Smith, A global positioning system–based climatology for the total electron content in the ionosphere, Journal of Geophysical Research: Space Physics. 115 (2010) A10318.

[14] W. Wan, F. Ding, Z. Ren, M. Zhang, L. Liu, B. Ning, Modeling the global ionospheric total electron content with empirical orthogonal function analysis, Science China Technological Sciences. 55 (2012) 1161–1168.

[15] A.J. Coster, J.C. Foster, P.J. Erickson, Monitoring the ionosphere with GPS, GPS World. 14 (2003).

[16] Z. Liu, Y. Gao, Ionospheric TEC predictions over a local area GPS reference network, GPS Solutions. 8 (2004) 23–29.

[17] A. Vernon, L.R. Cander, Regional GPS receiver networks for monitoring local mid-latitude total electron content, Annals of Geophysics. 45 (2002) 649–656.

[18] D. Okoh, O. Owolabi, C. Ekechukwu, O. Folarin, G. Arhiwo, J. Agbo, S. Bolaji, B. Rabiu, A regional GNSS-VTEC model over Nigeria using neural networks: A novel approach, Geodesy and Geodynamics. 7 (2016) 19–31.

[19] R.F. Leandro, M.C. Santos, A neural network approach for regional vertical total electron content modelling, Studia Geophysica et Geodaetica. 51 (2007) 279–292. https://doi.org/10.1007/s11200-007-0015-6.

[20] M. Ding, A neural network model for predicting weighted mean temperature,

Journal of Geodesy. 92 (2018) 1187–1198.

[21] S. Pereira, P. Canhoto, R. Salgado, M.J. Costa, Development of an ANN based corrective algorithm of the operational ECMWF global horizontal irradiation forecasts, Solar Energy. 185 (2019) 387–405.

[22] A. Manzato, A. Pucillo, A. Cicogna, Improving ECMWF-based 6-hours maximum rain using instability indices and neural networks, Atmospheric Research. 217 (2019) 184–197.

[23] M.O. Selbesoglu, Prediction of tropospheric wet delay by an artificial neural network model based on meteorological and GNSS data, Engineering Science and Technology, an International Journal. 23 (2020) 967–972.

[24] M.J. Homam, Prediction of total electron content of the ionosphere using neural network, Jurnal Teknologi. 78 (2016).

[25] L. Mallika I, D.V. Ratnam, S. Raman, G. Sivavaraprasad, Performance analysis of Neural Networks with IRI-2016 and IRI-2012 models over Indian low-latitude GPS stations, Astrophysics and Space Science. 365 (2020) 1–14.

[26] URL-1, International GNSS Service, (n.d.). https://igs.org/ (accessed January 31, 2022).

[27] URL-2, TUSAGA-Aktif, (n.d.). https://www.tusaga-aktif.gov.tr/ (accessed January 31, 2022).

[28] URL-3, GPS-TEC analysis software, (n.d.). http://seemala.blogspot.com (accessed January 31, 2022).

[29] M.A. Sharifi, S. Farzaneh, Local Ionospheric Modeling Using the Localized Global Ionospheric Map and Terrestrial GPS, Acta Geophysica. 64 (2016) 237–252.

[30] Y. Norsuzila, M. Abdullah, M. Ismail, Leveling Process of Total Electron Content(TEC) Using Malaysian Global Positioning System(GPS) Data, American Journal of Engineering and Applied Sciences. 1 (2008).

[31] Y. Xiang, Y. Gao, An enhanced mapping function with ionospheric varying height, Remote Sensing. 11 (2019) 1497.

[32] L.R. Cander, M.M. Milosavljevic, S.S. Stankovic, S. Tomasevic, Ionospheric forecasting technique by artificial neural network, Electronics Letters. 34 (1998) 1573–1574.

[33] R.F. Leandro, M.C. Santos, Comparison between autoregressive model and neural network for forecasting space environment parameters, Bollettino Di Geodesia e Scienze Affini. 63 (2004) 197–212.

[34] T. Kohonen, Adaptive, associative, and self-organizing functions in neural computing, Applied Optics. 26 (1987) 4910–4918.

[35] P.K. Simpson, Artificial Neural Systems: Foundations Paradigms, Pergamon Press, New York, 1990.

[36] URL-5, World Data Center SILSO, (n.d.). https://wwwbis.sidc.be/silso/ (accessed January 31, 2022).

[37] H. Jin, T. Maruyama, 3-3-2 Different behaviors of TEC and NmF2 observed during large geomagnetic storms, Journal of the National Institute of Information and Communications Technology Vol. 56 (2009).

[38] R. Leitinger, L. Ciraolo, L. Kersley, S.S. Kouris, P. Spalla, Relations between electron contentand peak density: regular and extreme behaviour, Annals of Geophysics. 47 (2004).

[39] URL-4, Community Coordinated Modeling Center (CCMC), (n.d.). https://ccmc.gsfc.nasa.gov (accessed January 31, 2022).

[40] A.J. Conway, K.P. Macpherson, G. Blacklaw, J.C. Brown, A neural network prediction of solar cycle 23, Journal of Geophysical Research: Space Physics. 103 (1998) 29733–29742.

[41] M.R.G. Razin, B. Voosoghi, A. Mohammadzadeh, Efficiency of artificial neural networks in map of total electron content over Iran, Acta Geodaetica et Geophysica. 51 (2016) 541–555. https://doi.org/10.1007/s40328-015-0143-3.

[42] E. Tulunay, E.T. Senalp, L.R. Cander, Y.K. Tulunay, A.H. Bilge, E. Mizrahi, S.S. Kouris, N. Jakowski, Development of algorithms and software for forecasting, nowcasting and variability of TEC, Annals of Geophysics. 47 (2004) 1201–1214.

Supplementary Material Link:

https://github.com/aliozk4n/Supplementary_Material.git